Analysis of the Geometrical Properties of Packed Beds, and Their Influence on Effective Diffusion and Hydrodynamic Dispersion

Siarhei Khirevich, Alexandra Höltzel, and Ulrich Tallarek

Department of Chemistry, Philipps-Universität Marburg, Hans-Meerwein-Strasse, 35032 Marburg, Germany
e-mail: khirevich@gmail.com, tallarek@staff.uni-marburg.de

Introduction

Quantification of the transport processes in packed chromatographic columns based on the column pore space geometry is a long-standing topic in chromatography, and has been addressed via simulations and experimental studies. This topic is crucial on the way to understand, and, therefore, control and optimize the packing process of chromatographic columns which is now considered an art rather than a science. The complexity of the column packing procedure as well as resulting column pore space makes it very difficult to perform systematic experimental studies of transport in the columns, and computer simulations are the only possibility to perform such studies. In this work we generate isotropic periodic random sphere packings of equal-sized spheres over wide range of porosities (between random close and random lose packing limits) using six packing protocols, and perform accurate transport simulations in the packing void space utilizing high-performance computing facilities.

We analyze pore space of the generated packings using spatial tessellations and provide scalar geometrical descriptors which are i) independent on the packing generation protocol (i.e., can be applied for *any* sphere packing) and ii) in strong correlation with the effective diffusion and hydrodynamic dispersion coefficients. Our results demonstrate strong influence of the generation protocol on transport coefficients, and, as a result, that the packing porosity cannot be used as the only parameter characterizing transport in the chromatographic columns.

Packing generation

We generated packings of randomly-packed equal-sized (monodisperse) spheres using Jodrey–Tory and Monte Carlo-based algorithms. The generated packings are periodic, isotropic, and have dimensions of $10d_p \times 10d_p \times 70d_p$ (d_p is the sphere diameter), which is sufficient for performing both statistical analysis of packing microstructure and accurate simulation of transport (flow, diffusion, hydrodynamic dispersion) within the packing void space.

JT algorithm randomly distributes sphere centers in the simulation domain and iteratively removes overlaps between spheres by spreading apart of two closest sphere centers on each iteration. The initial random arrangement of sphere centers, the magnitude of closest pair displacement, and packing porosity (ε, void space fraction) define the *degree of heterogeneity* (DoH) of the final packing microstructure (Figures 1 and 2). Due to generation procedure, JT packings have the microstructure significantly different from the one of MC random packings (for the description of algorithm see captions of Figures 3 and 4).

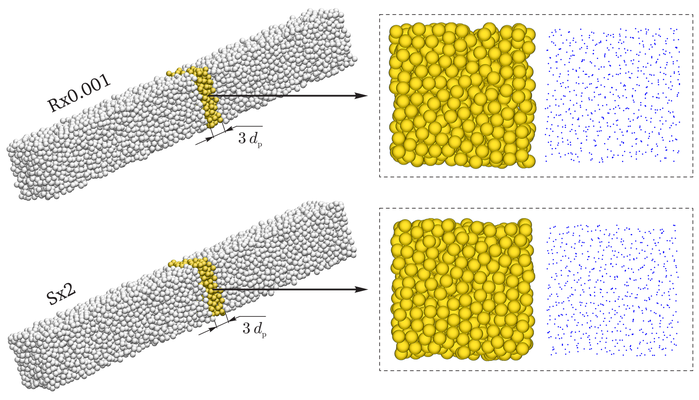

Figure 1. Unconfined random sphere packings at the random-loose packing limit (ε = 0.46) of two types Rx0.001 and Sx2. Shown are packing side views (left), sections of three particle layers as a front view (center) and corresponding projections of particle centers onto the front plane (right). Differences between the two packing types are not discernible. Therefore, we use 2D disks to illustrate the differences between packing types (Figure 2).

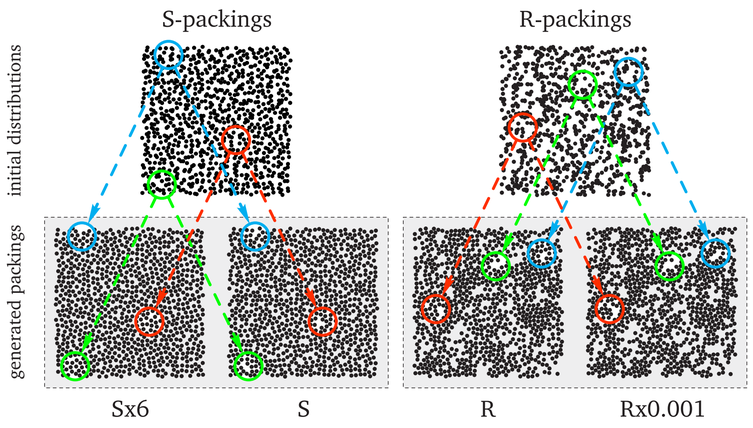

Figure 2. Random packings of monosized hard disks at ε = 0.46 generated with different packing protocols. Disks are used instead of spheres for better illustration of the difference between packing types. Generated packings are referred to as "TxM", where "T" is the initial distribution type and "M" is the magnitude of displacement (for M = 1, packings are referred to as just "T"). Figure shows the initial distributions of the disks for S- and R-types (top) and the generated packings (bottom). R-packings originate from a random uniform initial distribution of disk centers in the simulation box. To generate S-packings, the simulation box is divided into n equal cubic cells (n is the amount of disks) and each disk center is placed in a random position into a cell. Both R- ans S-types result in a uniform random distribution of disk centers within the simulation box. Magnitude of displacement M determines if the initial distribution of disks is preserved (small M) or significantly altered (large M). Color circles help to compare the microstructure in the initial distribution and in the generated packing.

MC algorithm locates all spheres on a dilute simple cubic lattice in the expanded simulation box (Figure 3). On each iteration, MC moves each sphere a short distance in a random direction and rejects moves resulting in a sphere overlap. The simulation box is compressed during generation (with rate Ω) until its original dimensions are obtained.

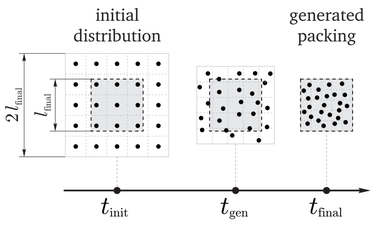

Figure 3. Schematic representation of MC algorithm. Left: initial distribution of disks (spheres in 3D) in ordered lattice; simulation box is expanded. Middle: random moves of each disk, no overlaps are allowed. Right: generated packing.

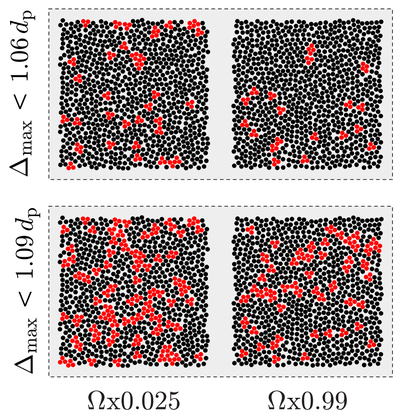

Figure 4. Effect of the compression rate value Ω on the microstructure of bulk random packings of monosized disks at ε = 0.34 generated with a Monte Carlo procedure. Closely packed regions are colored in red. Closely packed disks form close-to-regular triangles on a Delaunay mesh (resulting from connecting the centers of adjacent disks, see also Figure 8), and were identified by the value of the maximum edge length Δ_{max} of the triangles, with $\Delta_{max} < 1.06\ d_p$ (top), or $\Delta_{max} < 1.09\ d_p$ (bottom); d_p denotes the disk diameter.

Hydrodynamic dispersion

We employed lattice Boltzmann and Random Walk Particle Tracking methods to simulate flow and hydrodynamic dispersion in the generated packings. Chosen numerical approach allowed us to obtain both transient (Figure 5a) and asymptotic dispersion (Figure 5b,c) coefficients with high accuracy. Variation of the packing heterogeneity resulted in wide range of the obtained dispersion coefficients, and consequently very good agreement of our data with various simulated and experimental data available in the literature (Figure 5b,c).

Wide range of the obtained dispersion coefficients is confirmed by the *geometrical* analysis of generated packings (performed using Voronoi tessellation, see Figure 9): statistical moments of the distribution of Voronoi volumes (Figure 5d,e) capture packing heterogeneity of different packing types and reflect their dispersion coefficients.

Finally, dispersion coefficients were simulated for the wide range of reduced velocities (Figure 6), and successfully fitted with the generalized Giddings' equation.

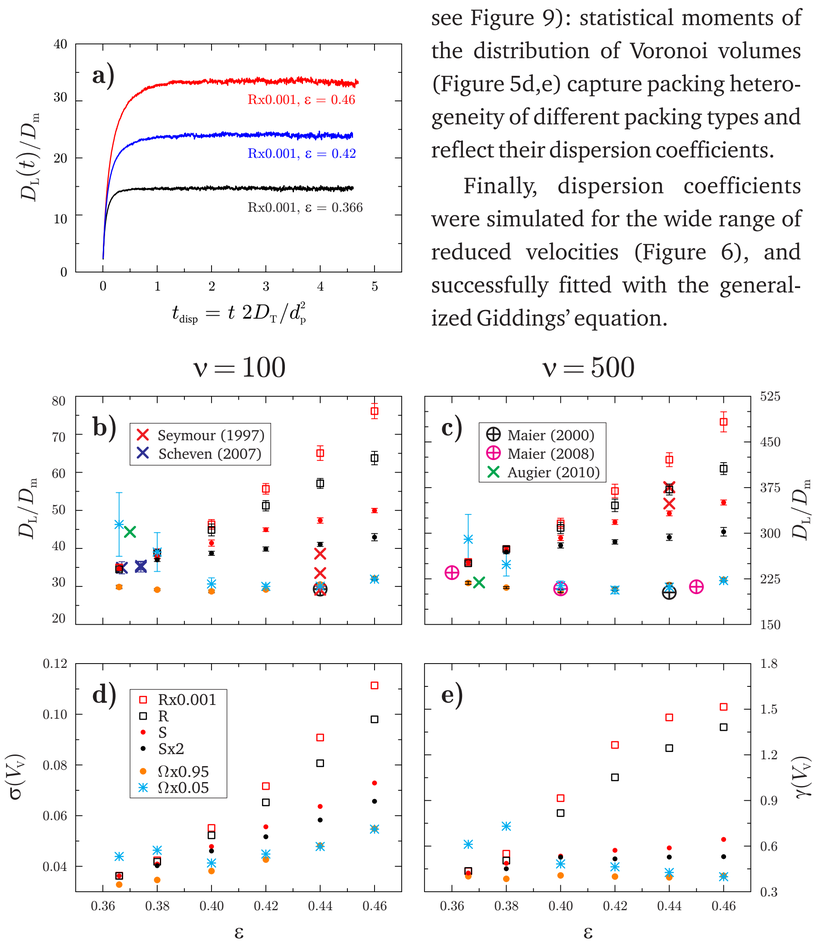

Figure 5. a) Hydrodynamic dispersion coefficient vs. dispersive time (D_T is asymptotic transverse dispersion coefficient). **b,c)** Asymptotic values of the dispersion coefficients for ν = 100, 500. Comparison with literature data: NMR measurements of Seymour (1997) and Scheven (2007), and simulations of Maier (2000,2008) and Augier (2010). **d,e)** Statistical moments (standard deviation σ and skewness γ) of the probability distribution function of Voronoi volumes in generated packings.

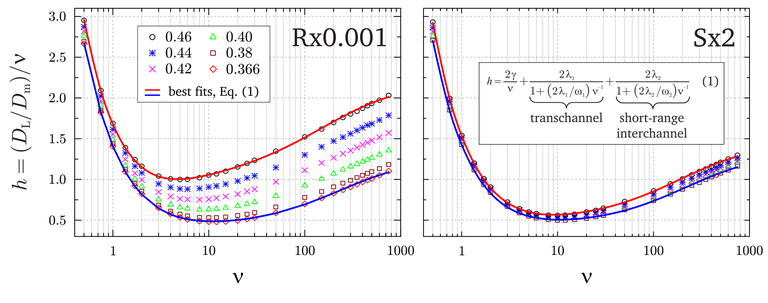

Figure 6. Reduced plate height values for heterogenous (Rx0.001) and homogenous (Sx2) packings. Values are obtained for wide range of reduced velocities, ν = 0.5–750, and fitted with the generalized Giddings' equation containing only transchannel and short-range interchannel terms.

Effective diffusion

Effective diffusion coefficients $D_{eff} = D(t\to\infty)/D_m$ were simulated using random walk particle tracking method. Use of this method in a combination with supercomputing facilities allowed us to a) track time evolution of the diffusion coefficient up to asymptotic limit (Figure 7a), and b) obtain *accurate* values of the asymptotic (effective) diffusion coefficient: see comparison with analytical solution in Figure 7b. Further, geometry of the packings was analyzed using Delaunay and Voronoi spatial tessellations. The idea behind this analysis is to divide packing pore space into a set of simple geometrical elements, analyze geometry of these elements, and find suitable geometrical descriptors which correlate with the effective diffusion coefficients (or tortuosity values). Figure 8 shows an empirically found geometrical descriptor originating from the Delaunay tessellation, while Figure 9 is dedicated to the Voronoi tessellation-based descriptor which is derived using basic results from the integral geometry (Benichou (2005)), and demonstrates a strong *anti*-correlation with *all* diffusion coefficients of random and crystal packings.

Figure 7. Simulated values of the diffusion coefficients ($D(t)$, D_{eff}) or tortuosity (τ). **a)** transient behavior vs. diffusive time. **b)** influence of the packing generation protocol and porosity on the asymptotic values of tortuosity; comparison with analytical solution for ordered packings. **c)** influence of sphere size distribution on tortuosity (R-type packings were generated using polydisperse spheres), and comparison with experimental data from the literature.

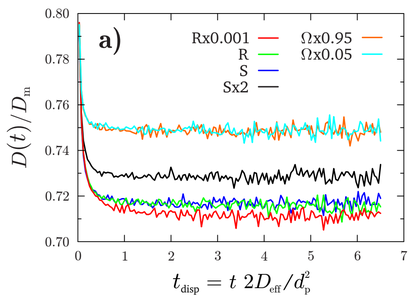

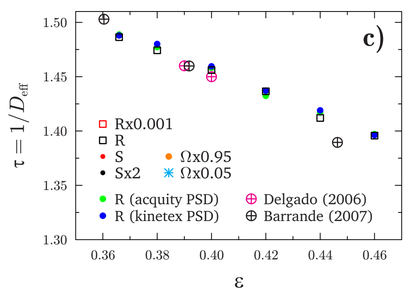

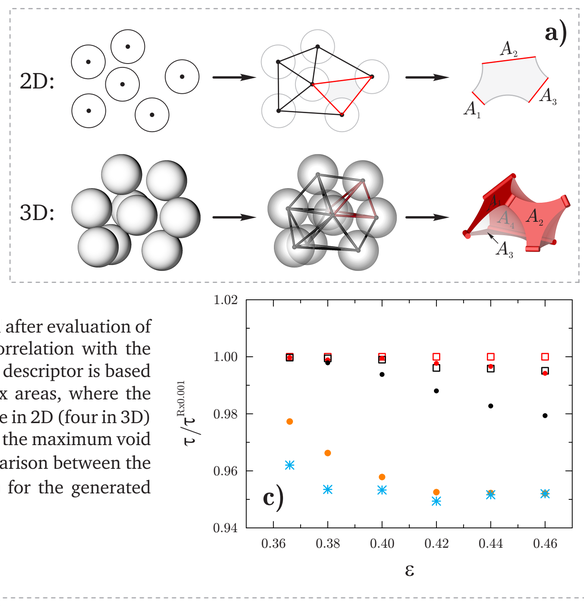

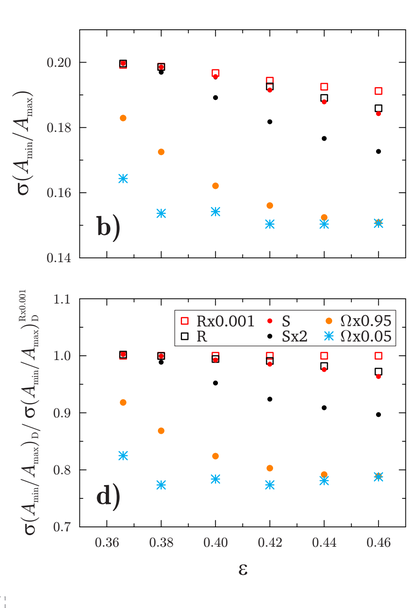

Figure 8. Geometrical analysis of the generated packings based on the Delaunay spatial tessellation of the packing pore space. **a)** Schematic illustration of the Delaunay tessellation in 2D (top) and 3D (bottom): centers of randomly located disks (spheres) can be interconnected with links dividing packing pore space without gaps and overlaps into a set of simplexes (triangles in 2D and tetrahedra in 3D). An individual simplex (indicated by the red links in the middle panel) as well as its faces contain both space points of the pore and of the spheres forming this simplex. In case of impermeable spheres diffusion occurs only in the void space of each simplex and through the void part of its faces. Right part of the panel a) visualizes a void part of a simplex together with its free faces indicated by A_i. Shape of each simplex as well as its void part can be characterized in different ways, and after evaluation of several geometric descriptors we found one demonstrating a strong correlation with the simulated tortuosity values of *random* (JT and MC) sphere packings. The descriptor is based on the ratio of the minimum (A_{min}) to the maximum (A_{max}) *free* simplex areas, where the corresponding limiting values are calculated for each simplex from its three in 2D (four in 3D) faces. **b)** standard deviation of the ratio between the minimum (A_{min}) and the maximum void face area (A_{max}) of each Delaunay tetrahedron around a pore. **c,d)** Comparison between the porosity-scaling of the tortuosity and geometric descriptor $\sigma(A_{min}/A_{max})$ for the generated packing types. Data are shown normalized to the Rx0.001-packing type.

Figure 9. Geometrical analysis of sphere packings based on the Voronoi tessellation. **a)** Schematic illustration of the Voronoi tessellation in 2D (top) and 3D (bottom). Middle panel: yellow polyhedra indicates Voronoi region of the green disk (sphere in 3D), and contains space points closer to this disk than to any of its neighbors. Gray shaded region denoted as the sub-Voronoi region is the contribution of one of the green disk neighbors to the Voronoi region. Right panel: sub-Voronoi region is formed by free (S_{free}) and solid (S_{solid}) boundaries. Using basic results from the integral geometry (Bénichou (2005)), the following geometrical descriptor can be derived:

$$M = \left\langle \frac{V^i}{\langle V^i \rangle} \cdot \frac{S^i_{free} + S^i_{solid}}{S^i_{free}} \right\rangle$$

where V^i is the volume and $S^i_{free,solid}$ is the free and solid surfaces of i-th sub-Voronoi region in a packing, and chevrons denote averaging over all sub-Voronoi regions in each generated random sphere packing. **b)** Dependence of the geometrical descriptor M on the porosity and packing type. Comparing the values of M with tortuosity values shown Figure 7b, a strong *anti*-correlation can be seen for *all* packings types, i.e. for generated random packings as well as ordered body-centered and face-centered cubic crystals (BCC and FCC).

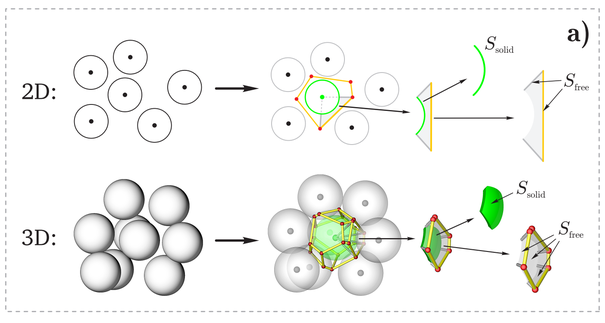

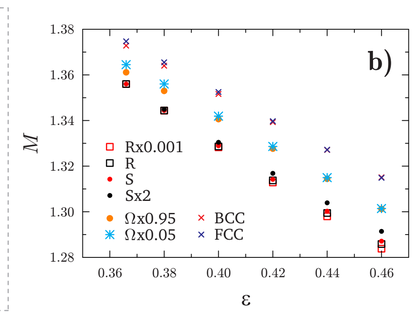

Conclusion

In this study we performed simulations of the effective diffusion and hydrodynamic dispersion in ordered (crystal) and random sphere packings generated at different porosity values. Employed numerical approach resulted in an accurate determination of the transient and asymptotic transport coefficients. Use of different packing types resulted in collecting a wide range of the transport coefficients, observation of excellent agreement with experimental, numerical, and analytical results from other studies, and making the following analysis of the pore space *independent* on the packing type. The pore space was analyzed with Delaunay and Voronoi spatial tessellations: using coordinates of spheres, the pore space is divided into a set of simple geometrical elements, shape of each element is quantified, and based on the values of individual elements the resulting scalar geometrical descriptor is derived. Different nature of the diffusion and hydrodynamic dispersion processes resulted in correlation with different geometrical descriptors. Descriptors shown in Figures 5d,e and 8b are found empirically, while the one in Figure 9b is based on the results from integral geometry. Therefore, we believe the approach presented here establishes a systematic route towards quantitative structure–transport relationships.

Acknowledgments

Computational resources on IBM BlueGene/P platforms were provided by "Genius" at RZG (Rechenzentrum Garching, Germany) and "Jugene" at FZJ (Forschungszentrum Jülich, Germany). We are grateful to the Jülich Supercomputing Centre (JSC) for allocation of a special CPU-time grant (project HMR10).

References

Augier, F.; Idoux, F.; Delenne, J. Y. *Chem. Eng. Sci.*, **65**: 1055–1064, 2010.
Barrande, M.; Bouchet, R.; Denoyel, R. *Anal. Chem.*, **79**: 9115–9121, 2007.
Bénichou, M. et al. *Europhys. Lett.*, **70**: 42–48, 2005.
Delgado, J. M. P. Q. *Can. J. Chem. Eng.*, **84**: 651–655, 2006.
Giddings, J. C. *Dynamics of chromatography: principles and theory.* Marcel Dekker, 1965.
Maier, R. S. et al. *Phys. Fluids*, **12**: 2065-2079, 2000.
Maier, R. S. et al. *Water Resour. Res.*, **44**: W06S03, 2008.
Scheven U. M.; Harris R.; Johns M. L. *Phys. Rev. Lett.*, **99**: 054502, 2007.
Seymour, J. D.; Callaghan, P. T. *AIChE J.*, **43**: 2096–2111, 1997.
Venema, P. et al. *J. Colloid Interface Sci.*, **141**: 360–373, 1999.